



Low-Velocity Impact Response of Nacre-Inspired E-Glass/Epoxy Composites With Varying Platelet Sizes

B. M. Vaghasia¹ | N. V. Rachchh¹ | Gaurang Joshi¹ | Dhanesh G. Mohan²

¹Department of Mechanical Engineering, Marwadi University, Rajkot, India | ²School of Computer Science and Engineering, University of Sunderland, England, UK

Correspondence: Dhanesh G. Mohan (dhanesh.mohan@sunderland.ac.uk)

Received: 20 May 2025 | Revised: 31 July 2025 | Accepted: 10 August 2025

Funding: This work was supported by the Marwadi University Minor Research Project Fund.

Keywords: bioinspired composite | low velocity impact strength | nacre-inspired platelet

ABSTRACT

This study explores the low-velocity impact behavior of nacre-inspired biomimetic platelet composites (NIBPC), using low-cost E-glass fiber in chopped strand mat (CSM) form as reinforcement and epoxy resin as the matrix. Platelet-shaped reinforcements of varying sizes (10, 15, 20, 25, and 30 mm) were precisely fabricated using a CO, laser cutting process. Composite laminates were manufactured through compression molding, consisting of five layers: outer layers made of triaxial mat and inner layers formed with randomly oriented nacre-like platelets. A monolithic nonbiomimetic laminate with five layers of CSM served as the reference. To evaluate the effect of platelet size on impact performance, drop-weight impact tests were conducted under controlled conditions using specimens of identical dimensions. The results reveal that NIBPC laminates outperform the reference laminates in terms of peak impact force and energy absorption. The 20 mm platelet configuration demonstrated the highest performance, achieving an impact energy absorption of 43.73 J, an 8.78% improvement over the reference laminate's 40.2 J, and a peak resistance force of 8431.45 N, representing a 24.34% increase over the reference value of 6780.61 N. Both visual inspection at the macrolevel and SEM analysis at the microlevel reveal the progressive variation in damage severity with changes in platelet size. The specimen with a 20 mm platelet exhibited the least visible damage at the macroscale, along with minimal delamination and crack dimensions at the microscale. The alignment between the two inspection methods confirms the enhanced ability of the bioinspired laminate to resist deformation under low-velocity impact loading. These findings highlight the critical role of platelet geometry in enhancing the toughness of bioinspired composites. The improved impact performance makes NIBPC materials promising candidates for automotive applications such as crash boxes, bumper beams, and engine bottom plates, where high energy absorption and durability are essential.

1 | Introduction

1.1 | Background of Bioinspired Material Capability

Many natural materials have been improved by nature over millions of years, and they often contain superior properties in certain areas that are difficult to achieve with artificial synthetic materials. Such natural materials are a combination of several basic components combined in several layers to form a hierarchical composite structure, and the mechanical and dynamic strength of the composite structure is often superior to a single-phase constituent [1–6] and significant improvement in low-velocity impact performance and damage resistance mechanism of bioinspired composite material with different helicoidal configurations recently observed by

This is an open access article under the terms of the Creative Commons Attribution License, which permits use, distribution and reproduction in any medium, provided the original work is properly cited.

© 2025 The Author(s). Polymer Composites published by Wiley Periodicals LLC on behalf of Society of Plastics Engineers.

Deng et al. [7]. Recently, Dura et al. [8] utilized bioinspired principles to develop fish scales-like composite laminate. Both experimental and numerical methodologies were used to enhance impact resistance by a 15.1% increase in resistance with higher scale volume and a 39.4% improvement from greater overlap ratios obtained. Chen et al. [9] developed hybrid fiber helical lay-up laminate (HHL) inspired by the helical structure of mantis shrimp dactyl clubs to improve ballistic resistance by light gas gun impact tests. Studies reveal that HHL contained 49.5% higher ballistic limiting velocity than traditional carbon fiber lay-up laminate. The performance improved at a 90° interlaminar helix angle, which promotes fiber engagement in dissipating projectile energy for advanced bioinspired composites.

1.2 | Mechanical Performance of Various Bioinspired Composite Material

Liu et al. [10] conducted a comprehensive review highlighting the importance of energy-absorbing (EA) designs to improve the crashworthiness of composite fuselage materials in aviation. Their study covered various composite configurations—such as tubes, corrugated plates, and bioinspired structures—and emphasized their ability to dissipate impact energy during crashes, thereby reducing the probability of structural failure.

In a related work, Liu et al. [11] reviewed different bioinspired metal composites fabricated through melt infiltration into porous reinforcement scaffolds. These materials replicate complex hierarchical architectures found in nature, enhancing toughness and damage resistance by minimizing crack propagation. One notable example includes the fabrication of Al/Al_2O_3 composites using zirconium acetate (ZRA) in icetemplating, which promotes tunable architectures and improves bending strength, compressive strength, and fracture toughness—making them suitable for metal-ceramic engineering applications [12].

Nurazzi et al. [13] presented a comprehensive review on the use of marine waste, particularly, seashells, as reinforcing agents in polymer composites. These seashell-derived calcium carbonate (CaCO₃) fillers improve the mechanical performance of polymer matrix laminates, while also offering potential for eco-friendly and sustainable engineering solutions.

Tran Thi Thu et al. [14] developed bioinspired helicoid laminated composite (B-iHLC) shells to evaluate dynamic impact responses under explosive loads. Their study demonstrated improved energy absorption and enhanced structural resilience, relevant for both military and civil infrastructure applications. Similarly, nature-inspired "mad structures" have shown potential for optimizing impact resistance and energy absorption by leveraging structure–function relationships, resulting in increased durability and multifunctionality in engineered materials [15, 16].

Ahamed et al. [17] investigated nacre-inspired engineered cementitious composite (NECC) beams subjected to quasi-static and dynamic bending loads. Their findings revealed superior

energy absorption capabilities compared to conventional monolithic structures—up to 195% improvement under quasistatic loading and 27% under dynamic conditions—achieved through layered and staggered configurations. Adopting such nacre-like hierarchical architectures has also shown promise in enhancing ballistic performance and penetration resistance [18].

Xu et al. [19] introduced a nacre-inspired $\operatorname{Ag-SnO}_2$ contact material with a layered hierarchical design, demonstrating improved erosion and impact resistance, along with self-repairing capabilities and effective stress distribution. These properties make such laminates suitable for extreme-condition electrical contact applications.

Wu et al. [20] developed a ceramic/polyurea staggered composite structure (CPSCS) based on a nacre-inspired design. Using ceramic surface modification, the structure displayed improved ballistic resistance against secondary projectile impacts. Similarly, Garg et al. [21] reviewed bioinspired materials that replicate hierarchical microstructures—such as helicoidal, sandwich, and nacre-like architectures—found in nature. These materials, inspired by nacre, fish scales, and arthropod exoskeletons, significantly improve impact resistance and prevent catastrophic failure modes.

An advanced nacre-based composite integrating shear-stiffening gel within a montmorillonite-MXene network reduced the transmitted force from 1308.1 to 370.4 N, outperforming traditional engineering materials [22]. Likewise, bulk Cu/reduced graphene oxide (Cu/rGO) composites with a nacre-like hierarchical structure, fabricated via spark plasma sintering (SPS), showed a \sim 67% increase in compressive strength and \sim 19% increase in ductility compared to nonbiomimetic Cu/rGO laminates [23].

Finally, Chu et al. [24] addressed corrosion resistance in magnesium (Mg) alloys by developing an inverse nacre-inspired waterborne coating. Their system, based on polyvinyl alcohol/glutaraldehyde (PVA/GA) and graphene oxide/glutaraldehyde (GO/GA) matrices, combined with heat treatment, enhanced hydrophobicity in rGO sheets. The resulting "maze effect" provided a stable and effective corrosion protection barrier.

1.3 | Impact Performance of Nacre Inspired Composite Laminate

Wei et al. [25] designed hybrid laminate structures inspired by natural biomaterials like nacre, conch shell, and mantis shrimp dactyl clubs, which improve energy absorption capacity by 375% compared to basic structures, and proposed a unique coupling of brick-mud and lamellar structure. These notions reveal that a combination of soft phase volume and hybridization of architectures can improve toughness and stiffness for high-performance protective materials. Wu et al. [26] performed the optimization of nacre-like composites by nondominated sorting genetic algorithm II (NSGA-II) optimization technique with objective functions for parameters like tablet shape, dimensions, and mechanical properties to balance toughness and strength. The result reveals that penetration depth was reduced by 31.61%, wave-staggered laminate

improved the ballistic limit by 27.21%, and energy absorption capacity improved by 8.3% compared to conventional block plates. Jargalsaikhan et al. [27] investigated freeze-casted bioinspired nacre-like alumina (Al₂O₂)-based composites to improve ceramic dental crowns' flexural strength and toughness by incorporating multilayer Al2O3 with different polymer phases. The study shows that the nacre mimic composite distributes stress effectively, and polymer layers act as stressrelieving zones that undergo plastic deformation to reduce stress concentration, leading to cost-effective composite structures that exhibit significant potential for applications in dental crown materials. Yuan et al. [28] introduced the fractional approach by generalizing Taylor's formula to model the dynamic behavior of meso-discontinuous media in oyster shells (nacre-based species). By use of finite element methods, the relationship between equivalent fractional order and fractal dimension effectively analyzes the impact of porous structures during wave propagation. CO2 pulse laser testing revealed that denser nacre, having meso-discontinuous brick-mud structure, gives wave attenuation and velocity reduction compared to chalk material. Zeng et al. [29] developed a biomimic nacre-like composite film for sustainable food packaging through the layered structure of natural nacre using cellulose nanofibrils, nanocrystals, montmorillonite, polyvinyl alcohol, and alkyl ketene dimer. Their findings provide oxygen and water vapor transmission rates and significant resistance to oil and water by surpassing conventional biodegradability. This notion provides the potential of nacre-based layered composites to offer eco-friendly, durable material, which replaces petroleum-based packaging. Huang et al. [30] explored a nacre-inspired MXene/polyurethane (MP) nanocomposite film to improve the mechanical properties, like tensile strength of 298.02 MPa, toughness of 13.81 MJ m⁻³, electromagnetic interference shielding (48 dB) achieved, which is higher than Kapton films for potential low Earth orbit (LEO) applications. Nature-inspired soft composites with staggered architectures, mainly nacre-based composites, possess higher strength and toughness due to the staggered arrangement and resembling protein-matrix connections among mineral platelets that optimally dissipate fracture energy [31].

1.4 | Ballistic Performance of Various Nacre Mimic Composites

Wang et al. [32] propose layered-and-staggered concrete inspired by abalone shells (nacre outer shell), tested with Type 53 API bullets at high impact velocities and give superior ballistic resistance properties. Xiong et al. [33] implement a nacre-like microstructure design to enhance crack resistance in brittle material, simulate it through the distinct element method (DEM) with J-integral to estimate crack propagation, and measure fracture energy. Nacre replicates composite laminates that exhibit higher energy absorption and dissipation capacity during various impact loading events, such as low-velocity impact, high impulse load, blast conditioning, and ballistic load [34-38]. A comprehensive state-of-the-art review [39, 40] dedicated to nacre-inspired composite laminates reveals that a unique combination of hierarchical fiber-reinforced architectures offers remarkable mechanical properties, fracture toughness, and resilience. Mimicking "brick-and-mortar" and helicoidal

structures observed in nature has the potential to develop sustainable and robust engineering materials.

1.5 | Gap and Motivation

The majority of recent scholarly work has polarized on creating nacre-inspired composite laminates by utilizing costly reinforcement and matrix materials like graphene [23, 24], carbon fiber [9], Ag-SnO² [19], and metal oxide ceramic-based material [12, 18, 20, 26, 27, 37]. Additionally, it increases expenses for demanding fabrication process requirements and the environment leads to minimizing feasibility for widespread usage. Furthermore, limited attention has been drawn to the more affordable, feasible, and sustainable fabrication of nacre-inspired composites. Therefore, this work primarily focuses on the fabrication and testing of nacre-inspired E-glass/epoxy composite laminate, which includes low-cost E-glass fiber nacre-like platelets as reinforcement material embedded into epoxy resin that acts as a matrix material fabricated by an economic manual die compression molding process.

Additionally, recent studies reveal that the adaptation of biomimetic strategies inspired by nacre has garnered significant attention; however, a critical gap remains in understanding the influence of platelet size variation within nacre-inspired architectures, particularly, in the context of conventional fiberreinforced composites. Existing literature has primarily focused on advanced or nanoscale materials, while the application of E-glass fiber reinforcement combined with epoxy resin materials that are widely available, low-cost, and industrially scalable has not been adequately explored. This represents a key research gap, as most studies overlook the practical integration of nacre-like designs into affordable and commercially viable composite systems. Moreover, prior work has largely emphasized static mechanical characterization, with limited focus on dynamic mechanical performance, such as low velocity impact resistance, which is critical for real-world structural applications. To address these deficiencies, the present study adopts a nacre-inspired stacking strategy using varying platelet sizes within E-glass/epoxy laminates and demonstrates its significant enhancement in impact performance. This work not only introduces an original material-fabrication approach within the biomimetic paradigm but also extends the understanding of dynamic behavior in accessible composite systems.

The outline of this work is as follows: Section 2 contains the experimental methodology, which includes specimen geometry, fabrication procedure, and testing setup. Section 3 provides a comparison and discussion of the testing results. Finally, Section 4 includes the summary of the entire conclusion.

2 | Experiment Methodology and Materials

The NIBPC laminate is fabricated by a manual die compression molding process in which compressive force is applied with the help of an aluminum die male part with the help of a tightening screw up to the gap between the male and female parts to reach a 3.5 mm distance. A nonstretchable die made of aluminum grade 6031 material is capable of sustaining a maximum compressive



FIGURE 1 | Aluminum manual compression die with tightening screw closed setup.



FIGURE 2 | Female part of die with ejecting screw holes.



FIGURE 3 | CSM raw sheet.

load of up to 100 KN without any deformation and generating a smooth surface finish on the top and bottom faces of the laminate with the least irregularity. The compression molding process uniformly distributes the resin (epoxy) material throughout



FIGURE 4 | Laser cutting machine setup.

the die cavity, reinforcement material properly covered by matrix material without leaving any voids or air interruption, and uniform thickness (i.e., $3.55\,\mathrm{mm}$) obtained over an entire area of $300\times300\,\mathrm{mm}$. Figures 1 and 2 illustrate the closed-die setup, where Figure 1 shows the assembly with tightening screws, and Figure 2 depicts the female part containing a rectangular cavity with ejector screw holes.

E-glass fiber CSM (chopped strand mat) with a density of 450 GSM (grams per square meter) was utilized, and nacre-like platelet shapes of five different sizes (i.e., 10, 15, 20, 25, and 30 mm) were cut from the CSM sheet using a $\rm CO_2$ -based laser cutting machine. Figures 3–5 illustrate the raw E-glass fiber CSM sheet with dimensions of $\rm 300\times300\,mm$, nacre-like platelets in five different sizes, and the laser engraving and cutting machine setup used for fabrication.

A 2D nacre-inspired hexagonal polynomial-shaped platelet was designed using AutoCAD drafting software to ensure accuracy and precision in platelet geometry, which was then directly exported to "RD Works" for laser processing, laser cutting software that generates compatible G-code to guide the laser path followed by input G-code command. The accuracy of the laser machine calibrated up to 0.02 mm was maintained throughout the cutting operation. Table 1 reveals the cutting process parameters maintained during the entire nacre-inspired reinforcement material fabrication. These optimum parameters were obtained through trial and error to achieve better quality and quick production of nacre-inspired polynomial hexagonal shaped reinforcement. Different combinations of cutting speed (mm/min) and CO2 laser power intensity (% value) utilized to figure out the optimum parameters for fabrication of nacre-inspired platelet fabrication. Table 1 reveals the parameters used in the laser cutting process to fabricate the nacre-inspired platelet extracted from raw E-glass fiber CSM reinforcement material.

In the CO_2 based laser cutting process, key process parameters perform a critical role in obtaining the precision and quality of the cuts. The cutting speed value is $8\,\mathrm{mm/min}$, confirming a controlled and steady material removal rate. The source power values are calibrated with a maximum power percentage of 60% and a minimum power percentage of 50%, which gives an optimal balance between energy input and thermal impact on the reinforcement material during fabrication. In software



FIGURE 5 | Platelet size increased from 10 to 30 mm shaped by laser cutting process (left to right).

 $\begin{tabular}{lll} \textbf{TABLE 1} & \vdash & \textbf{Fixed input parameters used for laser-cutting nacre-like} \\ \textbf{platelets}. \\ \end{tabular}$

Sr. no.	Process parameters	Input value
1	Cutting speed (mm/min)	8
2	Maximum power percentage	60%
3	Minimum power percentage	50%
4	Process type	Cut

Note: All values were constant during fabrication and not subject to variation.

UI, the process type is set as "cut," indicating the process's nature is to remove the targeted portion of reinforcement material. Additional parameters like focal length, gas pressure, and nozzle diameter can be considered to enhance the comprehensiveness of the process. These parameters calibrated at the focal length of 50 mm can ensure precise intensity and stable delivery, while gas pressure is set to 5 bar with an additional gas, like a mixture of oxygen and nitrogen, utilized to enhance quality and minimize thermal stress. A fixed value of a nozzle diameter of 1 mm can further improve the process by ensuring a precise and concentrated laser beam.

Specimen geometry and size for NIBPC and nonbiomimetic plain composite (NBPC) laminate maintained as per ASTM D7136 standard, that is, $150\,\text{mm} \times 100\,\text{mm}$ (length \times width) and specimen thickness $3.55 \pm 0.04\,\text{mm}$ maintained throughout the

entire laminate. Lay-up stacking sequence for NIBPC laminate having the following arrangement where the top and bottom layers are made of triaxial mat [0°/+45°/-45°] and the middle three layers are made of E-glass fiber platelet with different configurations in terms of size. The nonbiomimetic plain laminate consists of two layers of triaxial mat and three layers of CSM, alternately stacked as illustrated in Figures 6 and 7. Both laminates (i.e., NIBPC, NBPC) contain a total of nine layers of reinforcement material having distinct middle layer configuration. Table 2 [41] represents individual material properties of E-glass fiber reinforcement and matrix material (epoxy resin).

Table 3 presents the assigned codes for both laminate configurations, that is, the bioinspired and plain laminates.

Figure 8 shows both the bioinspired laminate and the plain monolithic laminate after the curing process. The bioinspired platelets with varying side lengths are clearly visible due to the placement of the laminate in natural sunlight. The random orientation and size of the platelets are distinctly observable.

Low velocity drop weight impact machine employed for measuring out plan impact strength of NIBPC laminate as represented in Figure 9. This instrumented apparatus operates through a guided mass system, which maintains precise alignment and positioning of the impactor mass throughout the testing procedure. The system implements a rebound elimination mechanism to minimize the possibility of secondary impacts. Moreover, it

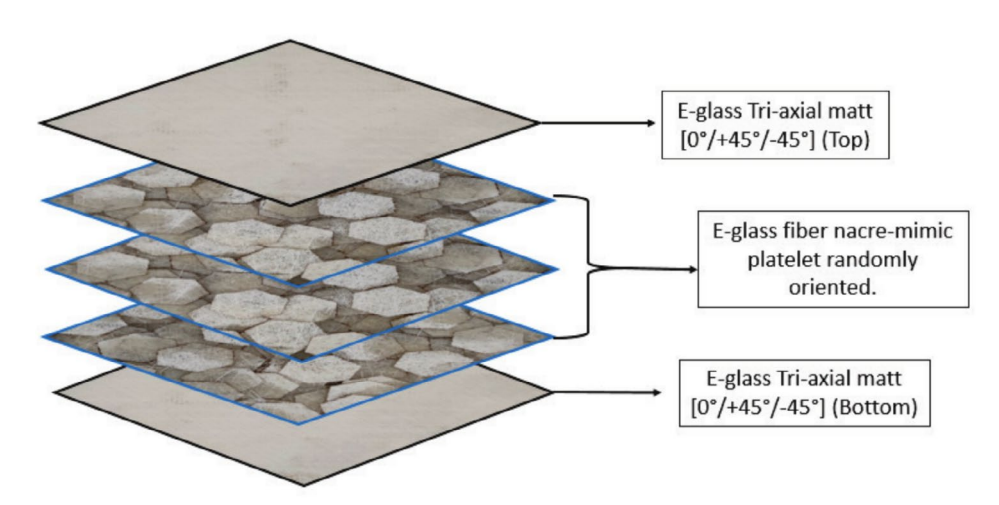


FIGURE 6 | Schematic illustration of the laminate lay-up sequence showing the stacking arrangement of triaxial mat and nacre-inspired platelet reinforcements of varying sizes.

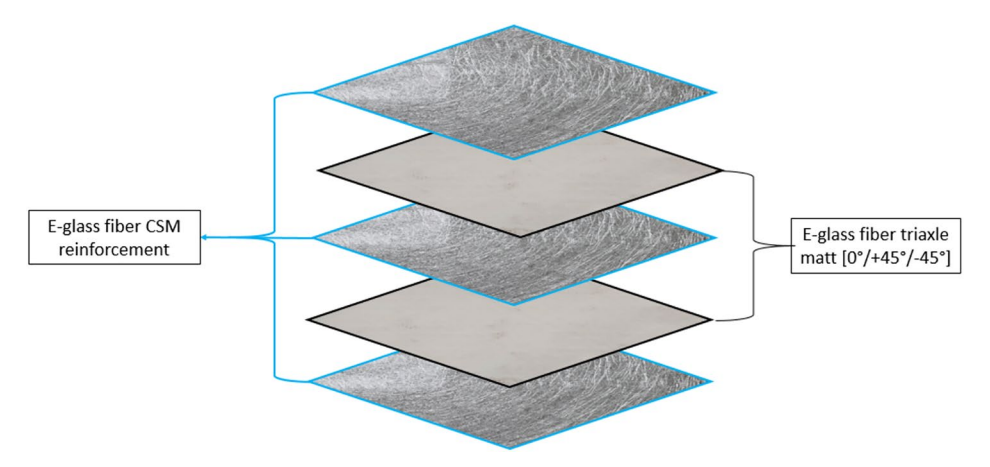


FIGURE 7 | Schematic illustration of the laminate lay-up sequence showing the stacking arrangement of triaxial mat and chopped strand mat (CSM) layers.

TABLE 2 | Individual constituent material properties chart [41].

Sr. no.	Material name	Density (g/cm ³)	Tensile modulus (GPa)	Tensile strength (MPa)
1	E-glass fiber	2.6	70	2000
2	Epoxy	1.8	3.5	70

TABLE 3 | Code assigned for bioinspired laminate and plain laminate configuration.

Code assigned	Platelet size (mm)		
E10	10		
E15	15		
E20	20		
E25	25		
E30	30		
T1	Plain laminate (nonbioinspired)		

introduces a robust holding mechanism that fulfills the standards ASTM D7136 requirement. These advanced facilities collectively capture the data with high accuracy and reproducibility in impact strength measurement. Furthermore, the initial impact energy is tuned by controlling two important testing parameters: the drop height ("h" unit meters) and the mass of the impactor. The machine's operations comprise parameters like control of height (meter), velocity (m/s), and energy (Joule) along with data acquisition (i.e., sampling rate) and data visualization system, which are managed through an integrated software interface through a connected personal computer.

Real-time measurement of the impact force is captured through a piezoelectric load cell, which is strategically located behind the impactor. This arrangement allows for accurate force measurement during the interaction between the impactor and the targeted area of the test specimen. The captured force and contact

time data are processed through a numerical integration method (i.e., trapezoidal method) to compute the area under the force versus time curves, which offers critical insights into the energy absorption characteristics of the tested material. An impactor that was hemisphere-shaped with a diameter of 16 mm, a drop height location of 0.42 m, and a mass of 9.8 kg was employed for this investigation. These parameters were meticulously maintained to deliver an impact energy of $40 \pm 0.1 \,\mathrm{J}$ with an impact velocity of approximately 2.9 m/s. A total of six samples (i.e., five NIBPC and one plain laminate) were prepared and subjected to impact testing under normal atmospheric conditions, following the guidelines outlined in ASTM D7136 [36]. These specimens were configured to explore the influence of varied parameters (i.e., bioinspired platelet size and nonbio mimic laminate) on their impact performance. During the fabrication stage, the gap between the male and female of the die is maintained at 3.5 mm to ensure uniformity in laminate thickness and proper distribution of matrix material throughout the laminate, which reduces variability due to differences in raw material distribution and consumption.

Furthermore, all specimens were fabricated under identical room temperature and allowed 48 h curing times, which eliminated potential inconsistencies in the fabrication process. Properly calibrated and well-maintained testing equipment was used. The calibration provides the precise and accurate measurement value of impact force, velocity, and absorbed energy, which minimizes errors in data acquisition and enhances the reliability of the experimental results.

3 | Result and Discussion

This section provides an analysis of the influence of bioinspired platelet size on the low-velocity impact performance of NIBPC laminates. The experimental results are illustrated as forcetime and energy-time curves corresponding to platelet sizes of 10, 15, 20, 25, and 30 mm and compared with a nonbiomimic laminate, having graph titles E10–E30 for NIBPC laminate and T1 for plain laminate material, which are shown in Figures 10 and 11. All these figures give representative curves for the tested specimens, which include maximum and minimum limits of the experimental data, offering a comprehensive perspective on the

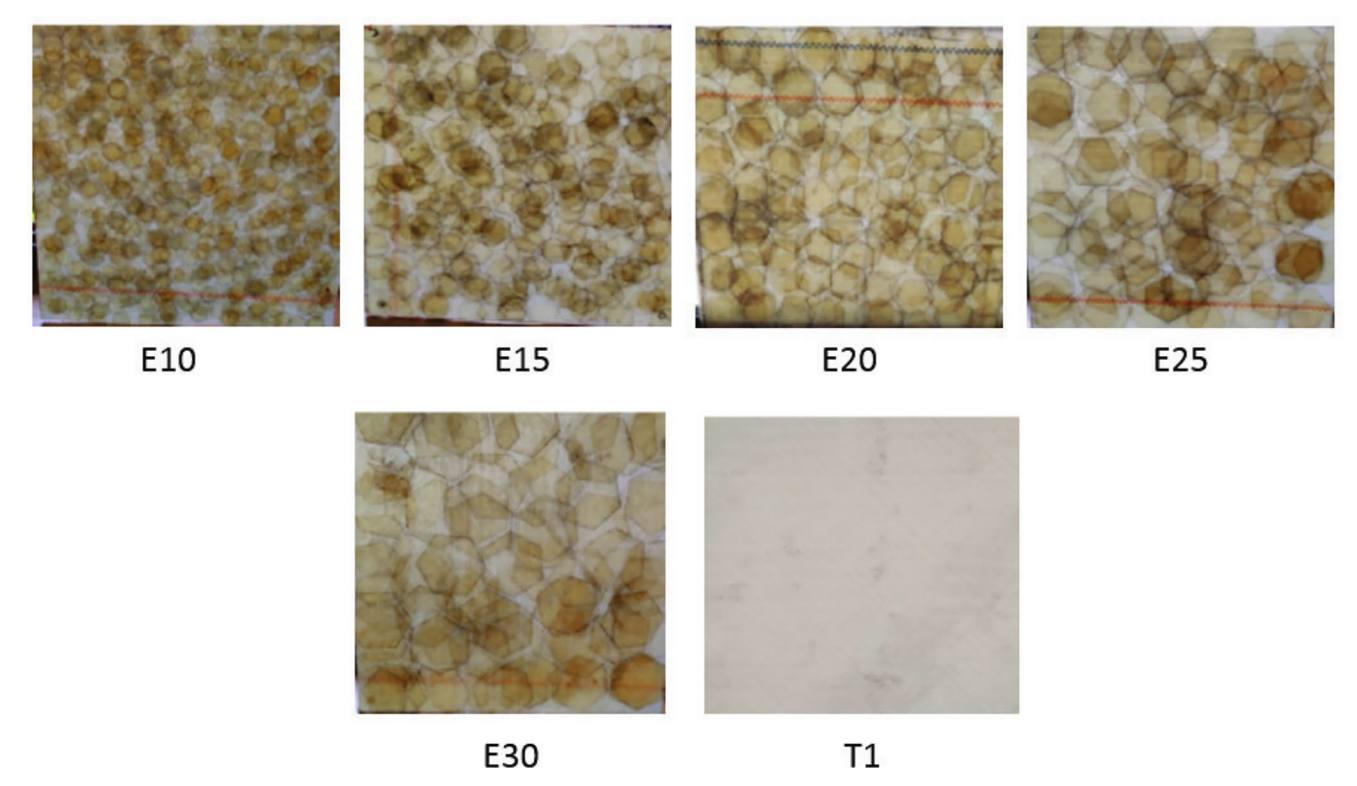


FIGURE 8 | Laminate after curing process, Code "E" assign for each NIBPC laminate and each number represent nacre inspired platelet size of reinforcement like E10 represent NIBPC laminate with platelet size 10 mm. T1 code assign for monolithic (nobioinspired laminate).

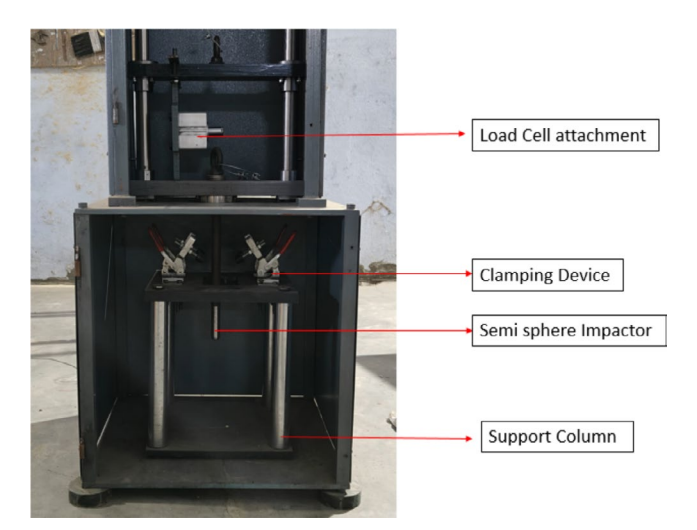


FIGURE 9 | Low-velocity impact machine setup.

variations in the impact response over different platelet sizes of bioinspired laminates.

Table 4 provides a quantitative summary of the maximum values obtained for key parameters, including absorbed energy, peak force value, contact time, and total displacement through the graphical representations. These measurements offer a clear and concise overview of the low-velocity impact response for each platelet size of NIBPC laminate and NBPC laminate, facilitating a direct comparison of performance across different configurations of laminate. The results for maximum force display major fluctuations across the different platelet sizes. However, no definitive trends related to the influence of the variation of

platelet size on these parameters are discernible. These variations are consistent with the changes in bioinspired platelet sizes observed in impact testing studies, which highlight the different impact behaviors associated with such studies. Recorded tabulated data, associated with the graphical insights, give a solid foundation for evaluating the effects of bioinspired platelet size on the impact performance of NIBPC laminate.

A one-way ANOVA test was conducted to compare the absorbed energy across various laminate configurations. The analysis revealed a statistically significant difference among the groups (F(5, 24) = 39.38, p < 0.001), indicating that platelet size has a substantial influence on impact energy absorption. The degrees of freedom between groups (5) and within groups (24) support the robustness of the analysis. Among all configurations, the E20 specimen exhibited the highest mean absorbed energy, and this finding is statistically supported by the ANOVA results. These results validate that the variation in platelet size significantly affects the dynamic performance of the nacre-inspired E-glass/epoxy laminates.

3.1 | Force Versus Time Behavior

The force versus time curve is shown in Figure 10, which exhibits different oscillatory patterns that lead to the vibrations induced in the specimens during the impact event [8, 42–44]. These vibration patterns result from the transient dynamic response induced by low-velocity impact, reflecting the differences in energy absorption, stress wave propagation, and damping behavior between the NIBPC and the NBPC laminates. The vibrational behavior captured in these curves paves critical insights into

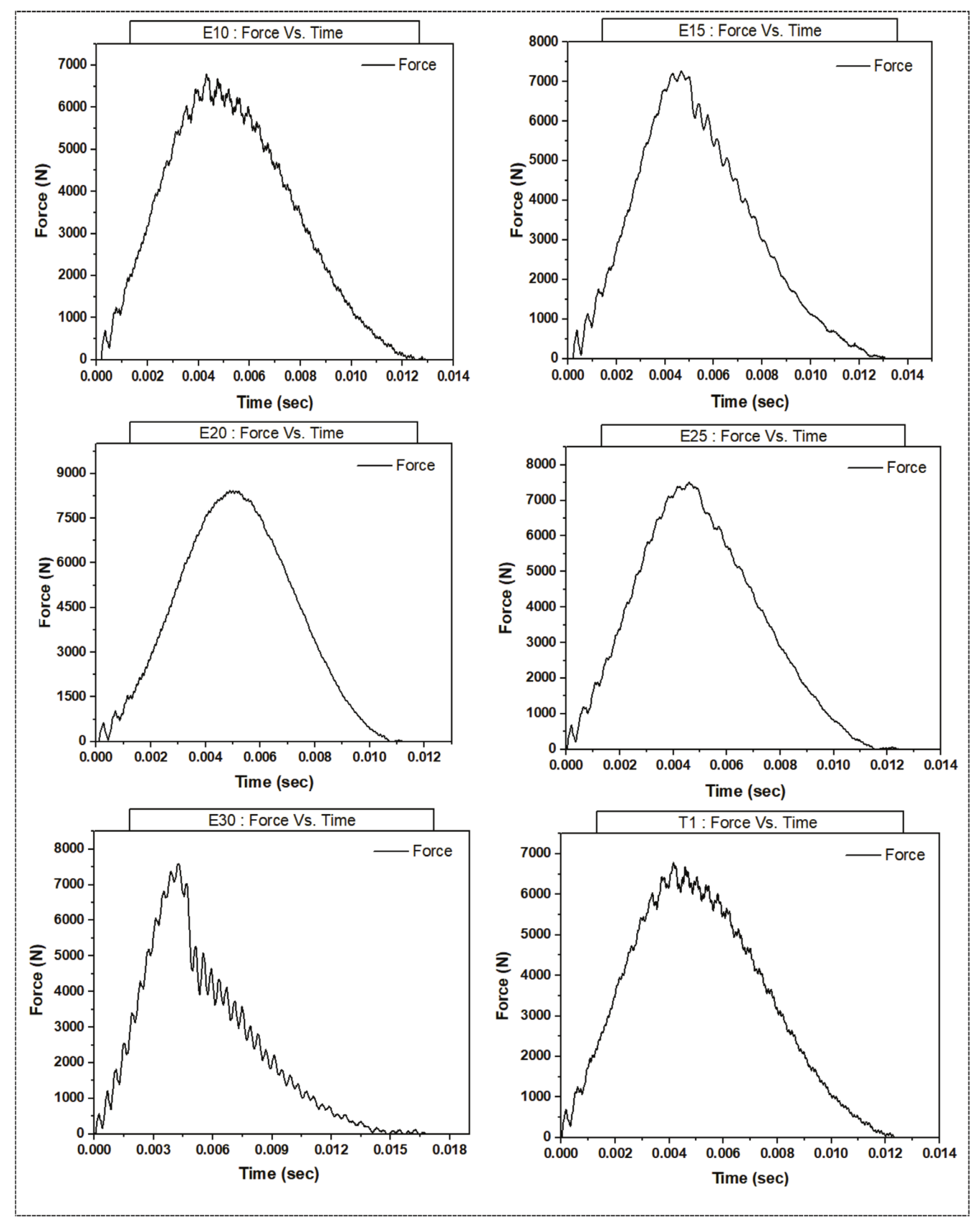


FIGURE 10 | Effect of platelet size on force versus time curve.

the dynamic mechanical properties of the laminates, like stiffness, damping properties, and energy absorption and dissipation mechanisms. Such information is crucial for understanding the

composites' performance and resilience under impact loading, enabling a complete evaluation of their structural integrity and suitability for practical applications.

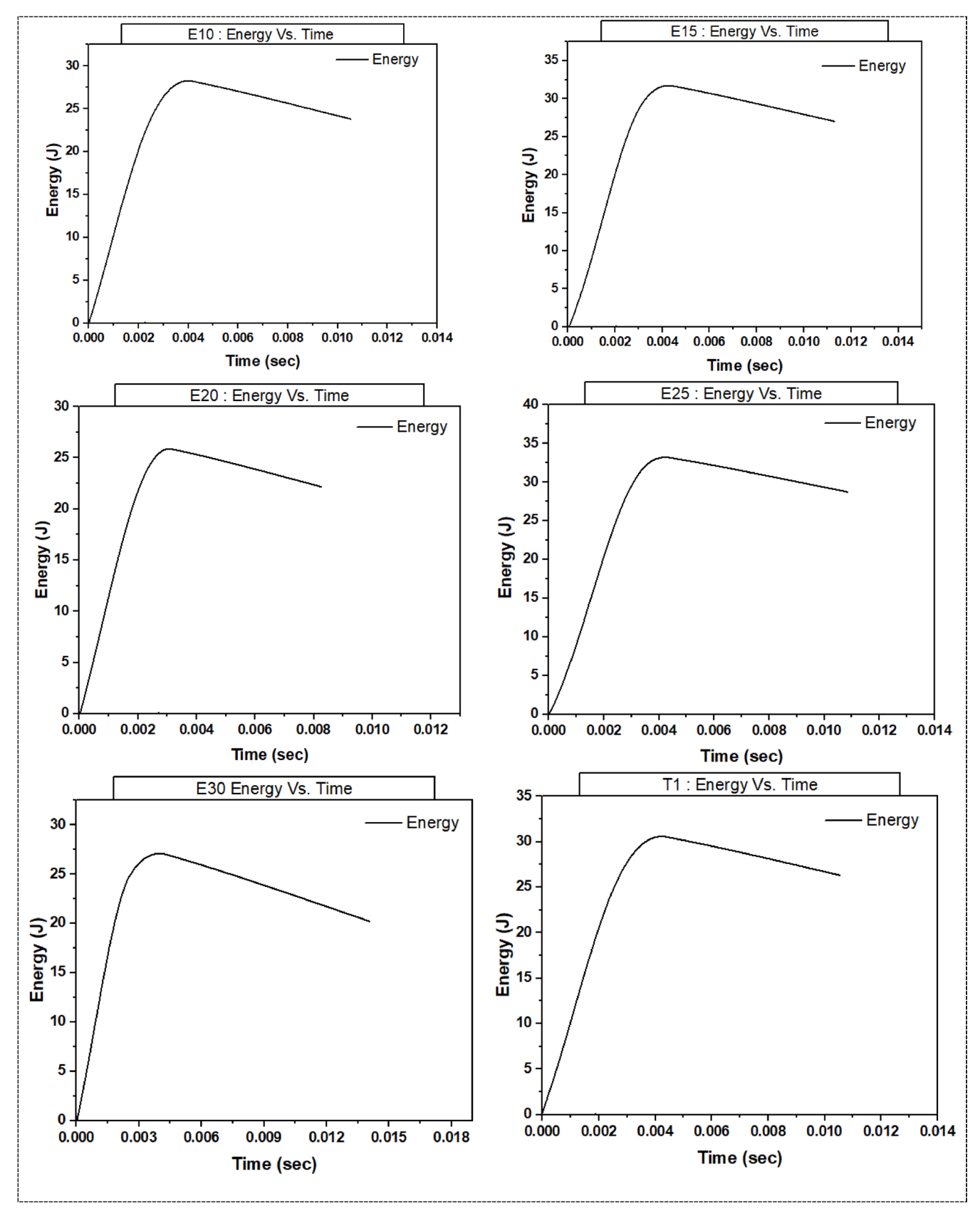


FIGURE 11 | Absorbed energy versus time curve of NIBPC and NBPC laminate.

Additionally, a distinct trend was observed in the value of frequency and amplitude during the unloading part of the curves from all specimens when the decay of the impact force

exhibited notable common behavior from Specimen Code E10 and T1, which indicates the same damping properties possessed by nacre-inspired material and plain monolithic

TABLE 4 | Impact performance of different laminate configurations.

Laminate code	Absorbed energy (J)	Peak force (N)	Contact time (ms)	Total displacement (mm)
E10	40.2 ± 0.6	6768.25 ± 115	12.92 ± 0.3	74.62 ± 1.8
E15	39.44 ± 0.7	7265.06 ± 135	13.30 ± 0.4	75.38 ± 2.0
E20	43.73 ± 0.5	8431.45 ± 140	11.20 ± 0.2	65.45 ± 1.5
E25	40.85 ± 0.6	7515.39 ± 125	12.46 ± 0.3	71.11 ± 1.7
E30	39.06 ± 0.8	7585.33 ± 130	16.78 ± 0.4	102.9 ± 2.5
T1	40.2 ± 0.5	6780.61 ± 110	12.44 ± 0.3	70.85 ± 1.6

Note: Values are expressed as mean \pm estimated standard deviation to illustrate expected variability. In actual testing, standard deviations would be derived from repeated experimental trials.

material. While increasing the size of platelet, the value of frequency and amplitude decreases and obtains the lowest value at platelet size 20 mm Code E20; after that, these dynamic properties further increase and reach a maximum value at platelet size 30 mm, as shown in the graph titled E30. This variation in vibration frequency and amplitude indicates the effect of nacre-like platelet size on the vibration properties of laminate, revealing the maximum damping properties obtained by laminate E20 having platelet size 20 mm, while a reversed trend is observed through further increasing platelet size from 25 to 30 mm. When compared with monolithic nonbioinspired material, nacre-like composite reflects the maximum damping properties and stiffness, indicating the ability of nacre-inspired platelets to distribute the impact force uniformly through their randomly oriented platelets and stacking sequence. Furthermore, the reduction in damping properties obtained through the increasing platelet size leads the material to behave as homogeneous and monolithic, which leads to a maximum value of frequency and amplitude inside the structure, which negatively affects the internal stiffness of the material.

Additionally, the pronounced difference in frequency and amplitude detected between the loading and unloading curves across all tests reflects the ability of nacre-inspired composite laminate to effectively absorb a significant portion of the imparted impact energy. This nature reveals the material's ability to dissipate energy by a synergy of various intrinsic damage mechanisms, like matrix fracture, fiber fracture, layer debonding, and fiber-matrix interfacial separation that showcase its potential for various applications requiring high energy absorption capacity. Furthermore, the concept of damping strength and rigidity in composite materials follows a series of irreversible alterations within the material during impact load, which is reflected in the form of energy dissipation. This behavior happened due to the heterogeneous hierarchical network of NIBPC laminate, characterized by the presence of randomly oriented platelet distribution and optimum size of platelet edges, allowing maximum energy dissipation by mitigating damage propagation through resisting fiber-matrix separation, interlayer fracture, and matrix failure. Various diverse strengthening mechanisms of NIBPC laminate promote an exceptional ability to absorb and distribute impact energy, which is vital for obtaining proper damping behavior and maintaining structural integrity through higher stiffness properties.

Moreover, a distinct and abrupt decline in impact force near its peak value was detected for all specimens, which indicates substantial damage initiation within both the NIBPC and NBPC laminate composite material. This sharp reduction in force can be obtained through the implementation of various failure mechanisms characteristic of the composite's internal structure. A detailed examination of the force-time responses further revealed that the value of this force drop, referred to as the gap size, progressively decreased with increasing platelet size from 10 to 20 mm, reaching a minimum gap at 20 mm platelet size (i.e., E20) after that, further increasing platelet size from 20 to 30mm, including NBPC laminate Coded T1, resulted in an increased gap size This phenomenon reveals the effect of nacreinspired platelet size influences the dominant damage response against impact loading and maximum resistance offered by the E20 specimen, while counter behavior observed for increasing platelet size (i.e., 20-30 mm) leads to decreasing damage response.

Additionally, no significant difference in force and time profile was observed in all specimens except specimen E20. During impact on the targeted surface, no dents or punctures were observed, which reflects the damage propagation significantly obtained by the mode of internal crack progression on the impacted surface. Following the impact, the rebound of the impactor resulted in a gradual decline in force values. The force-time curve for the E20 specimen demonstrated the highest peak force, characterized by a symmetric loading and unloading path. This behavior reflects greater elasticity and stiffness, contributing to a higher toughness value than other specimens.

3.2 | Energy vs. Time Behavior

Regarding Figure 11, the energy–time curves for NIBPC (E10 to E30) and NBPC (T1) laminates illustrate the typical low-velocity impact response which is generated by collecting force and time data captured through low-velocity impact testing machine. The maximum impact energy is associated with the synergistic combination of the slope of the ascending branch of the curve and the peak point which is followed by a gradual decline as the contact between the impactor and the specimen surface is lost. Once contact is terminated, the impacted energy stabilizes at a fixed value that indicates the energy dissipated by the specimens through various damage mechanisms (i.e., crack propagation). This dissipated energy is termed as "absorbed energy" and its significance

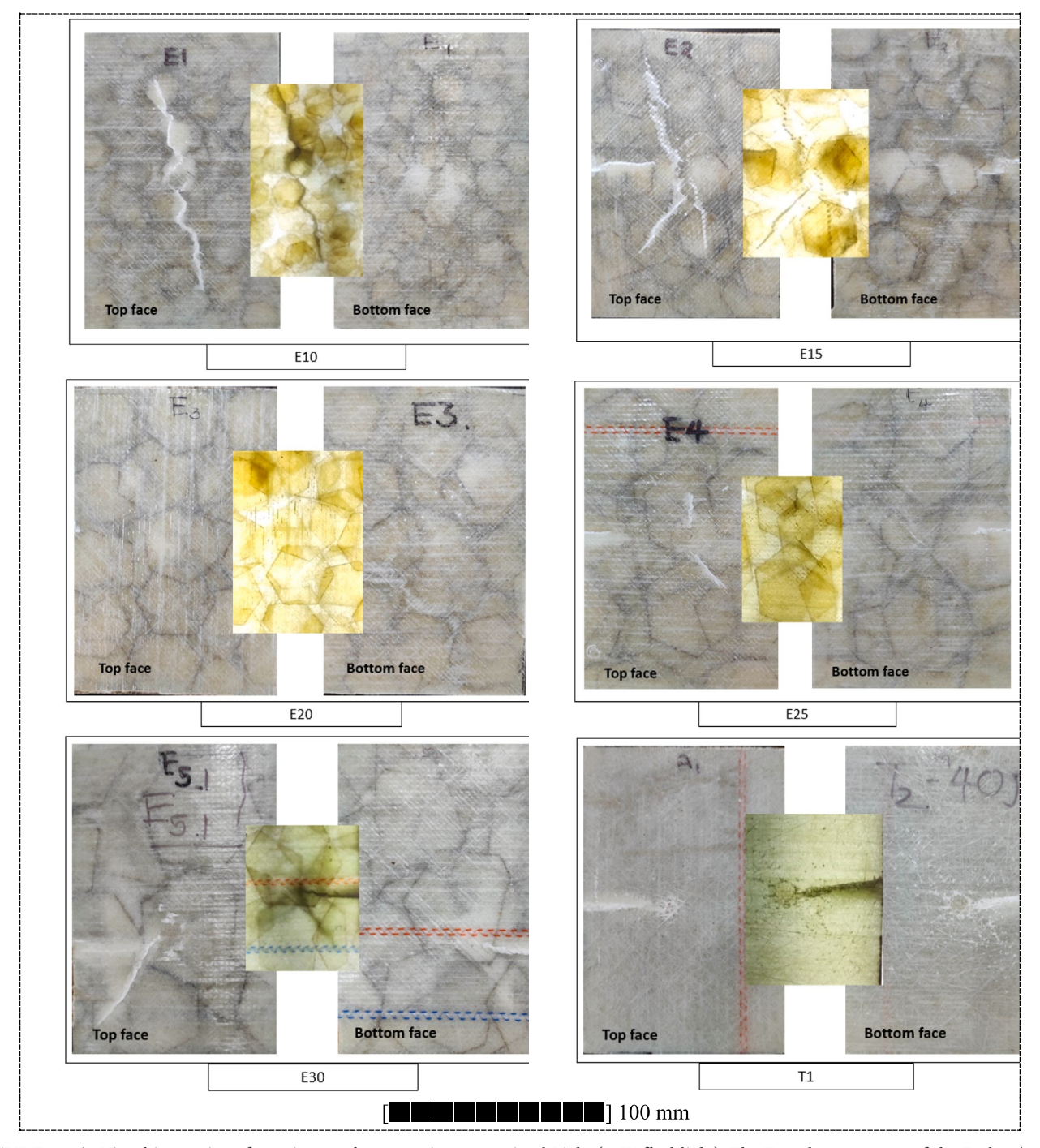


FIGURE 12 | Visual inspection of post-impact damage using transmitted Light (10 W flashlight). The Translucent nature of the E-glass/epoxy laminate enables observation of internal damage patterns. A scale bar is included for dimensional reference.

on damage severity is directly observed through visual inspection and computed radiography testing (i.e., Figures 12 and 13). Additionally, the portion of energy that remains undissipated during impact, which is temporarily stored by elastic deformation, is referred to as "elastic energy," quantified by the slope of the ascending curve. The total impact energy is the sum of the absorbed and elastic energy. This absorbed energy behavior with time curve (i.e., Figure 11) and Table 3 data indicate that increasing the nacreinspired platelet size (i.e., from 10 to 20 mm) initially enhances the slope of the elastic energy curve, reaching its maximum value at a platelet size of 20 mm. Beyond this size (i.e., 25–30 mm) the slope of the elastic energy curve declines sharply. Analysis based

on tabular data and graph reveals that the E20 laminate exhibits the optimum energy absorption capacity and dissipation capacity without leaving any significant cracks and damage on the laminate. Compared with monolith laminates, this signifies its superior toughness and impact resistance.

As the nacre-inspired platelet size increases up to 20 mm, a noticeable reduction is observed in the unloading pattern of the force-time curve, accompanied by the lowest absorbed energy values at this size. This reduction indicates that a smaller fraction of impact energy was dissipated as damage without crack propagation during the low-velocity impact event. In contrast,

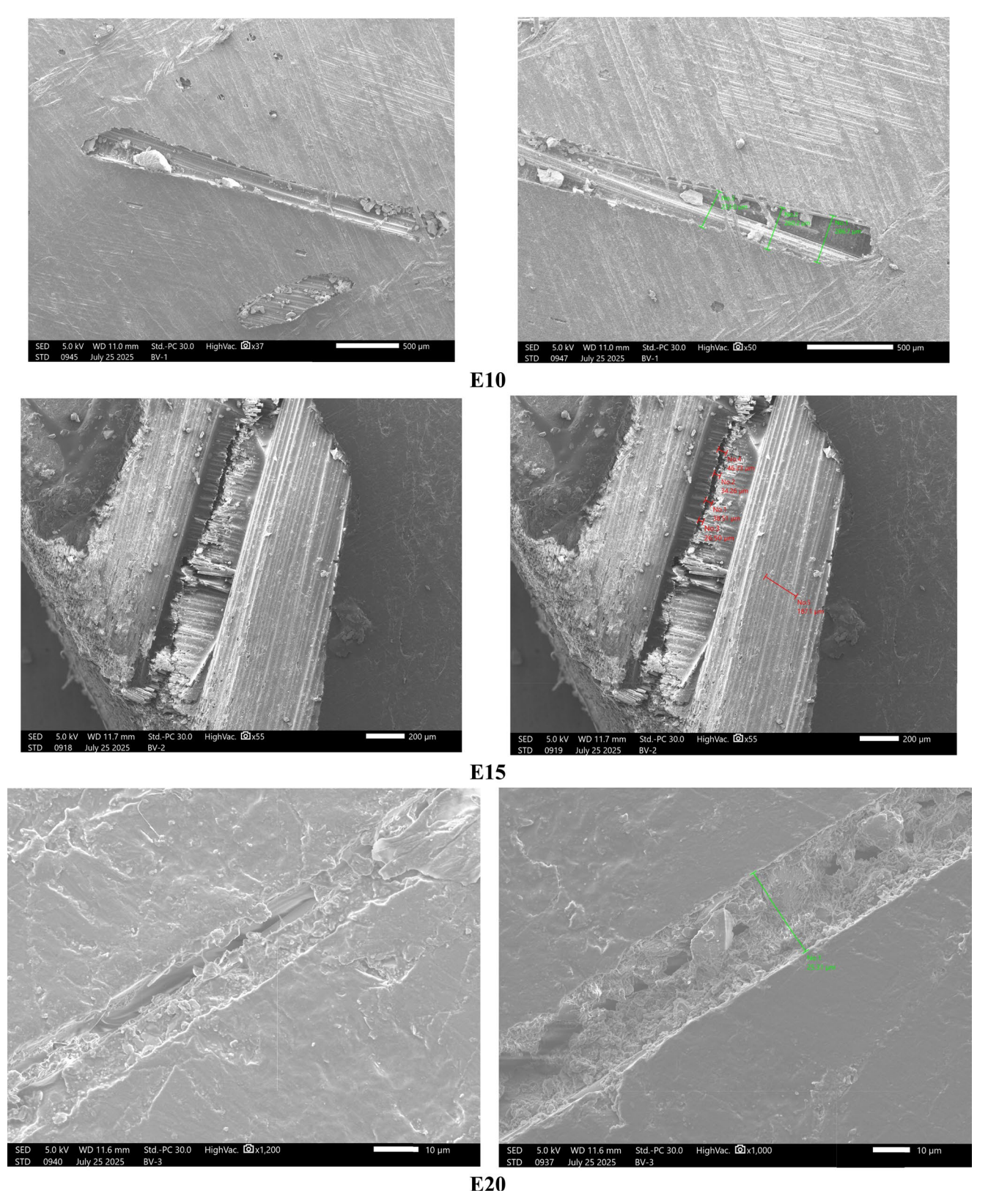


FIGURE 13 | SEM images of the damaged regions of bioinspired specimens (Codes E10–E30) and the nonbioinspired specimen (Code T1), showing the presence and dimensions of microcracks (indicated on the right side of each image).

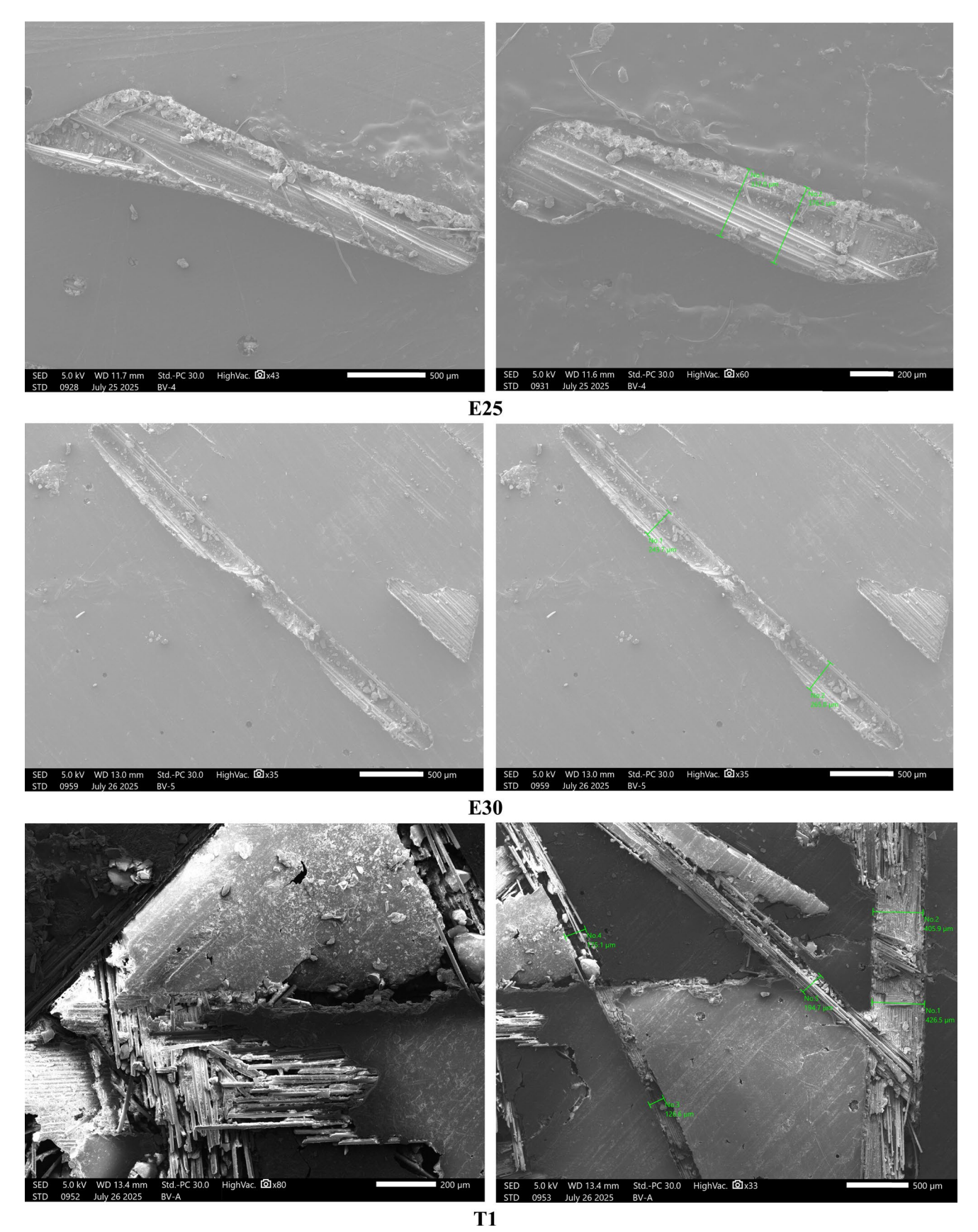


FIGURE 13 | (Continued)

the curves for other specimens, particularly, E30 and the monolithic material, exhibit higher peak values and a sharp decline, reflecting greater energy dissipation primarily through crack propagation mechanisms.

The absence of impact-induced deformation and less crack propagation are evident when comparing the externally visible damage across specimens (i.e., E10–E30) with different nacreinspired platelet sizes and the nonbioinspired monolithic composite material. This comparison is represented in Figure 12 which is obtained through a visual inspection method. These notions suggest that the NIBPC laminate demonstrates superior resistance to low-velocity impact loads compared to the NBPC laminate. Moreover, the visual observation reveals that the NIBPC laminate significantly enhances the specimens' ability to absorb energy through improving their overall elastic mechanical response.

3.3 | Visual Analysis Procedure

Along with the analysis of force and absorbed energy timeline, Figure 12 shows a visual analysis of the top and bottom surfaces of all impacted test specimens (i.e., E10–E20 and T1) provided further findings for the different visible damage modes obtained on specimens during testing. Visual analysis is an extensively utilized and standardized nondestructive testing (NDT) technique used in various industrial sectors, which include the aeronautic sector [45]. The various damage patterns that are externally visible on the impacted surfaces of specimens reveal the distinct levels of damage severity against impact load with different bioinspired platelet sizes (i.e., 10–30 mm) contained by the specimens.

From the visual observation, it clearly reveals the significant impact of platelet size on the intensity of damage in the tested specimens, which is directly supported by the force versus time and energy versus time graph. T1 specimen (i.e., NBPC laminate) depicted in Figure 12 indicates the significant crack propagation traveling from the impacted dent mark to the edge of the specimen which is clearly visible on the top and bottom surfaces of the T1 specimen. Yet, the impactor did not fully penetrate the specimens, but large crack lengths with platelet fiber breakage are observable. This phenomenon highlights severe internal damage to the NBPC laminate material compared to all NIBPC laminate. These various damage behaviors are coherent with the results extracted from the force-time and energy-time curves, which reinforce the capability of visual analysis to support quantitative data.

Comparatively, the specimens with 30 mm platelet size (i.e., E30), also illustrated in Figure 12, show the damage pattern (i.e., crack intensity) that is similar to that of the Specimen Code E25 but with a reduced severity as compared to T1, E10, and E15 specimens. The crack formation near the impacted location on the top faces is greater compared to the bottom faces for all types of specimens, except for the E20 specimen. The above notion highlights the improvement in impact resistance through adopting nacre-inspired platelets in composite laminate as compared to nonbioinspired composite laminate.

On the other hand, the specimens with platelet size 20 mm had a complete absence of any damage pattern observed, as illustrated in Figure 12. The top face and bottom surface exhibited a smooth texture without any single depression, puncture, or crack marked at the impact location throughout the entire surface area of the laminate. These impact responses on the surface reflect an almost zero severity of impact load on nacre-inspired platelet laminate with an optimum size of 20 mm, which indicates an enhancement of impact strength via uniform distribution of impact energy through elastic deformation over the entire laminate area.

Furthermore, increasing the platelet size from 10 to 20 mm shows a substantial reduction of crack length and zero at 20 mm size, which is clearly depicted in Figure 7. The impacted load response and crack severity progressively reduce with increasing platelet size up to 20 mm, at which the damage effect is zero without leaving any crack propagation footprint around the impacted surface region. These insights propose the significance of NIBPC laminate over NBPC laminate. Additionally, the effect of nacre-inspired platelet sizes on low-velocity impact performance depicts that the progressive increment of platelet sizes reaches optimum values of material toughness achieved; after that value, the impact strength is reduced by a further increment of platelet size, which converts bioinspired material behavior to nonbioinspired material, and further increment of platelet size does not improve the impact damage resistance property.

The absorbed energy and time curve shown in Figure 11 and Table 4 synergistically reinforce these insights. It has been proven that impact damage intensity increases as the absorbed energy dissipates through an externally visible medium, such as dent formation, crack propagation, deboning of fiber matrix interface, and so forth [46-48]. Accordingly, the energy data depicted in Table 4 reveal that specimens with platelet sizes 10, 25 mm and T1 laminate contain similar absorbed energy of 100.5% (i.e., applied 40 J) with visible damage, and for platelet sizes of 15 and 30 mm, the absorbed energy is 98.6% with less visible crack. In contrast, specimens with a platelet size of 20 mm absorbed a maximum impact energy of 109% without any surface cracks or dent marks. These energy absorption mechanisms confirm the pattern observed in the visual inspection, where the intensity of crack propagation followed an inverted "V" trend with platelet size. Combined analysis of visual inspection and impact response curves depicts the variation of nacre-inspired platelet sizes significantly affecting the severity of damage through crack propagation in NIBPC laminate. These notions highlight the essential role of platelet size effect in evaluating the impact performance and long-term durability of such nacreinspired composite materials. Additionally, the notions focus on the importance of accounting for nacre-inspired platelet size variation when considering these bioinspired composites for use in industrial applications where high resistance to impact is a crucial requirement.

A plausible explanation of the observed behavior for the NIBPC laminates under impact loading conditions is the internal heterogeneous structure of nacre-inspired composite material having a superior tendency to dissipate impact load effectively without any significant damage intensity [49]. This

phenomenon supports the laminate by improving its overall mechanical dynamic and static strength [40]. Nacre-inspired platelets are responsible for reducing the crack length due to their interlocking hybrid brick-mortar structure [50]. Additionally, the nacre-inspired platelet specimens integrate top and bottom layers of reinforcement made of tri-axial matt, which configure a brick-mortar hierarchical structure to minimize the damage propagation inside the laminate [51].

The present study demonstrates that the E20 configuration, based on nacre-inspired platelet geometry, exhibits superior low-velocity impact resistance compared to both traditional and other bioinspired laminate designs. This conclusion is supported by force-time and energy-time responses, which indicate higher peak force, greater energy absorption, longer contact time, and lower impactor displacement, alongside reduced visible damage observed during visual inspection. These findings are consistent with previous studies on E-glass/epoxy systems, though the present work introduces a novel architectural modification through platelet size variation. For instance, Tran Thi Thu et al. [14] investigated helicoid laminated composites using E-glass fiber and reported improved dynamic performance; however, their approach did not involve platelet-based geometrical control. Similarly, Garg et al. [21] reviewed multiple bioinspired laminates using glass and polymer matrices, including sandwich and helicoidal structures, but did not explore the influence of platelet sizing in nacre-mimetic arrangements. Compared to these studies, the current work uniquely incorporates tunable platelet dimensions within a nacre-like stacking strategy, offering a new pathway for optimizing energy dissipation and damage tolerance. Unlike conventional E-glass laminates, where impact performance is primarily governed by fiber orientation and layer count, the synergistic interaction between matrix and platelet-reinforced layers in this study leads to enhanced load redistribution and crack arrest capabilities. This positions the current nacre-inspired Eglass/epoxy configuration, particularly, E20, as a promising and scalable solution for impact-critical composite applications.

The findings of this study have direct implications for material selection and structural design in automotive crash applications. The superior energy absorption and damage tolerance observed in the E20 configuration demonstrate the effectiveness of nacre-inspired architectures in mitigating impact forces—a critical requirement in crash-resistant components such as bumpers, door intrusion beams, and front-end structures. Compared to conventional laminates, the nacre-like platelet arrangement provides enhanced load redistribution and crackarresting capability, which can reduce sudden catastrophic failure during collisions. Moreover, the use of E-glass fiber and epoxy resin offers a cost-effective and scalable solution, making it suitable for mass-produced automotive parts. These benefits align with current automotive industry trends toward lightweight, high-performance, and damage-tolerant materials [52, 53]. Incorporating bioinspired stacking strategies such as those explored in this work could therefore inform future design methodologies aimed at improving crashworthiness without compromising material cost or processability.

The geometry, size, distribution pattern, and orientation of nacre-inspired platelets play a crucial role in optimizing both static mechanical properties and impact performance. These parameters can be effectively tuned to enhance the static and dynamic behavior of composite materials under various loading conditions. In the present study, the nacre-inspired platelet with a 20 mm size (Specimen Code E20) demonstrated the most favorable low-velocity impact performance. This configuration absorbed the highest impact energy (43 J) and exhibited the greatest peak resistance force (8431 N). Additionally, it recorded the shortest contact duration between the impactor and the specimen (11 ms) and the lowest impactor displacement (65 mm), indicating reduced deformation. These results suggest that the optimized platelet geometry in the E20 specimen, featuring a hierarchical interlocking structure, effectively resists deformation and dissipates energy efficiently, thereby minimizing damage propagation under low-velocity impact loading [54-57].

3.4 | Scanning Electron Microscopy (SEM) Result

SEM analysis was conducted using a JEOL 7100F-HR instrument, which offers a maximum magnification capacity of up to $\times 600,000$ and a resolution of 0.3 nm. The specimen was prepared in accordance with the platform dimensions of the instrument, shaped into a $17 \, \text{mm} \times 17 \, \text{mm}$ square block sectioned from the damaged region of the original sample using a water jet machining process. A gold coating with an approximate thickness of 0.2 nm was applied to the sample surface to enhance conductivity and imaging quality.

The SEM inspection results of all six specimens, as presented in Figure 13, clearly indicate the severity of material damage under the applied low-velocity impact event. The SEM inspection conducted on the damaged portions of the specimens revealed the severity of damage at the microstructural level and correlated well with observations from standard visual inspection. Crack regions in all specimens were analyzed at a magnification of $\times 1200$, covering a field of up to $100\,\mu m$, to assess the extent of microlevel damage. Among the bioinspired specimens, specimen E20 exhibited the smallest crack width of $25.1\,\mu m$, along with minimal fiber and matrix delamination. This suggests a more uniform distribution of impact load between the fiber and matrix phases.

In contrast, the nonbioinspired specimen T1 exhibited the highest degree of damage, characterized by complete fiber–matrix delamination and a maximum crack separation width of 426 μm . This indicates poor interfacial bonding and inadequate load transfer capacity, leading to significant crack propagation and reduced impact resistance.

Overall, the bioinspired specimens (Codes E10–E30) demonstrated lower damage severity compared to the conventional laminate (T1), owing to their heterogeneous architecture, which effectively distributes the impact load across the fiber–matrix interface. Specimen E20 exhibited optimal performance under low-velocity impact loading. Additionally, the analysis showed that increasing platelet size from 10 to 15 mm reduced crack length and damage, while further increases in platelet size (25–30 mm) resulted in decreased impact strength and increased

crack propagation. This behavior highlights the existence of an optimum platelet size that maximizes impact resistance.

architecture and impact performance is critical for designing durable composite materials for structural applications.

4 | Conclusion

This study evaluated the low-velocity impact performance of NIBPC laminates with varying Nacre-inspired platelet sizes (10–30 mm) and compared them with NBPC monolithic laminates. Both laminate types were fabricated using a combination of laser cutting for reinforcement and manual compression molding, following ASTM D7136 standards to ensure consistency in geometric dimensions and thickness.

The low-velocity impact tests, conducted using an instrumented drop-weight machine, enabled accurate assessment of forcetime and energy-time responses. Most specimens (E10, E15, E25, and E30) exhibited consistent trends up to the peak force, while specimen E20 showed a sharp slope in both force and energy curves, suggesting higher elastic energy storage. A steep drop near the peak force indicated significant damage across all specimens; however, specimen E20 showed enhanced toughness, as supported by its energy-time response. This behavior changed notably with platelet size: a decrease in the sharp force drop was observed up to E20, followed by a sharp increase in specimens E30 and T1, indicating convergence in the impact behavior of NIBPC and NBPC laminates at larger platelet sizes.

Variations in the damage mechanisms were observed through both SEM analysis and visual (macrolevel) inspection, including differences in crack length and dent intensity. At the microstructural level, SEM imaging revealed details such as fiber-matrix delamination and crack width, with specimen E20 exhibiting the smallest crack width and partial delamination. This indicates the material's effective capability to distribute impact load, which is strongly influenced by platelet size. Specimens with smaller platelets, such as E10, exhibited pronounced surface cracks and severe delamination, while specimen E15 showed reduced crack widths, reflecting improved damage resistance. The nonbioinspired control specimen (NBPC, Code T1) exhibited the most severe damage at both macro- and microlevels, with extensive fiber-matrix failure. Macroscopically, cracks were visible across both surfaces and were further highlighted under flashlight inspection. Microscopically, deep indentations and complete fiber pullout were observed via SEM. An increase in platelet size up to 20mm significantly enhanced energy absorption and damage resistance. However, further increases beyond 20 mm (i.e., 25 and 30 mm) resulted in a decline in performance, indicating a size-dependent trade-off in impact resistance.

The enhanced impact performance of the NIBPC laminates is attributed to the randomly distributed Nacre-inspired platelet network, which introduces a hierarchical reinforcement structure. This configuration likely improved interfacial bonding and reduced crack propagation, contributing to better damage tolerance.

Overall, the findings underscore the significance of platelet size in tuning the mechanical response of nacre-inspired composites. A deeper understanding of the interaction between platelet

Author Contributions

B. M. Vaghasia: conceptualization, investigation, writing – original draft, methodology, formal analysis, data curation. **N. V. Rachchh:** methodology, funding acquisition, writing – review and editing, writing – original draft, formal analysis, resources, visualization, software. **Gaurang Joshi:** investigation, methodology, writing – review and editing, formal analysis, resources. **Dhanesh G. Mohan:** methodology, validation, visualization, writing – review and editing, formal analysis, project administration, data curation, supervision, conceptualization.

Acknowledgments

This study was fully supported through the Marwadi University Minor Research Project Fund.

Conflicts of Interest

The authors declare no conflicts of interest.

Data Availability Statement

The data supporting this research work will be provided upon reasonable request.

References

- 1. A. Ghimire, Y. Y. Tsai, P. Y. Chen, and S. W. Chang, "Tunable Interface Hardening: Designing Tough Bio-Inspired Composites Through 3D Printing, Testing, and Computational Validation," *Composites Part B: Engineering* 215 (2021): 108754.
- 2. X. Gao, S. Qi, X. Kuang, Y. Su, J. Li, and D. Wang, "Fused Filament Fabrication of Polymer Materials: A Review of Interlayer Bond," *Additive Manufacturing* 37 (2021): 101658.
- 3. W. Ouyang, B. Gong, H. Wang, F. Scarpa, B. Su, and H. X. Peng, "Identifying Optimal Rotating Pitch Angles in Composites With Bouligand Structure," *Composites Communications* 23 (2021): 100602.
- 4. H. D. Espinosa, J. E. Rim, F. Barthelat, and M. J. Buehler, "Merger of Structure and Material in Nacre and Bone Perspectives on de Novo Biomimetic Materials," *Progress in Materials Science* 54, no. 8 (2009): 1059–1100.
- 5. Y. Chen, Y. Ma, Q. Yin, et al., "Advances in Mechanics of Hierarchical Composite Materials," *Composites Science and Technology* 214 (2021): 108970.
- 6. G. Tan, Q. Yu, Z. Liu, et al., "Compression Fatigue Properties and Damage Mechanisms of a Bioinspired Nacre-Like Ceramic-Polymer Composite," *Scripta Materialia* 203 (2021): 114089.
- 7. Y. Deng, H. Jiang, and Y. Ren, "Low-Velocity Impact Resistance Behaviors of Bionic Hybrid-Helicoidal Composite Laminates," *Composite Structures* 351 (2025): 118614.
- 8. H. B. Dura, P. J. Hazell, H. Wang, J. P. Escobedo-Diaz, and J. Wang, "Energy Absorption of Composite 3D-Printed Fish Scale Inspired Protective Structures Subjected to Low-Velocity Impact," *Composites Science and Technology* 255 (2024): 110725.
- 9. W. Chen, J. Liu, X. Cao, C. B. Li, Y. Li, and X. Li, "Study on Projectile Impact Resistance of Carbon-Glass Hybrid Bioinspired Helical Composite Laminate," *Materials Today Communications* 39 (2024): 108703.
- 10. X. Liu, C. Bai, X. Xi, et al., "Impact Response and Crashworthy Design of Composite Fuselage Structures: An Overview," *Progress in Aerospace Sciences* 148 (2024): 101002.

- 11. Y. Liu, B. Chen, Z. Liu, Z. Zhang, and R. O. Ritchie, "Bioinspired Interpenetrating-Phase Metal Composites," *Progress in Materials Science* 144 (2024): 101281.
- 12. M.-Q. Sun and P. Shen, "Tunable Architectures in Al/Al2O3 Composites for Enhanced Damage Tolerance Using Zirconium Acetate-Mediated Ice-Templating," *Materials & Design* 237 (2024): 112608.
- 13. M. N. Norizan, M. N. F. Norrrahim, M. H. Mulla, et al., "13—Mechanical Performance of Seashell-Reinforced Polymer Composites for Structural Applications," in *Polymer Composites Derived From Animal Sources*, ed. S. M. Sapuan, C. H. Azhari, and N. M. Nurazzi (Woodhead Publishing, 2024), 243–257.
- 14. T. Tran Thi Thu, T. N. Anh, H. N. Thi, and H. N. Thi, "Transient Response of Doubly-Curved Bio-Inspired Composite Shells Resting on Viscoelastic Foundation Subject to Blast Load Using Improved First-Order Shear Theory and Isogeometric Approach," *Defence Technology* 38 (2024): 171–193.
- 15. M. K. Ahamed, H. Wang, and P. J. Hazell, "From Biology to Biomimicry: Using Nature to Build Better Structures A Review," *Construction and Building Materials* 320 (2022): 126195.
- 16. W. Zhang, J. Xu, and T. X. Yu, "Dynamic Behaviors of Bio-Inspired Structures: Design, Mechanisms, and Models," *Engineering Structures* 265 (2022): 114490.
- 17. M. K. Ahamed, H. Wang, A. Ameri, and P. J. Hazell, "Nacre-Inspired Design of Engineered Cementitious Composite (ECC) Beams for Enhanced Impact Resistance and Energy Absorption," *Journal of Building Engineering* 78 (2023): 107687.
- 18. G. Wu, X. Wang, Y. Wang, et al., "Ballistic Properties of Bioinspired Nacre-Like Ceramic/Polyurea Staggered Composite Structures," *International Journal of Impact Engineering* 195 (2025): 105137.
- 19. C. Xu, K. Wen, Z. Wang, et al., "Nacre-Mimetic Alternating Architecture of AgSnO2 Contact: Highly-Efficient Synergistic Enhancement of In-Situ Self-Repairing Erosion Resistance and Naturally Evolving Impact Resistance," *Journal of Materiomics* 11, no. 1 (2025): 100914.
- 20. G. Wu, X. Wang, Y. Wang, et al., "Penetration Mechanics of Nacre-Like Ceramic/Polyurea Staggered Composite Structures Under Secondary Impact of Projectiles," *Thin-Walled Structures* 205 (2024): 112514.
- 21. A. Garg, A. Sharma, W. Zheng, and L. Li, "Dactyl Club and Nacre-Inspired Impact Resistant Behavior of Layered Structures: A Review of Present Trends and Prospects," *Materials Today Communications* 41 (2024): 110553.
- 22. Z. Li, S. Wang, W. Wang, et al., "Nacre-Inspired MMT-MXene Integrated Shear-Stiffening Gel Composites for Personal Safeguard and Multi-Functional Electronics," *Composites Part B: Engineering* 280 (2024): 111526.
- 23. F. Liu, X. Lu, G. Jin, W. Liu, and Y. Chen, "Bulk Graphene-Based Composites With Artificial Nacre-Like Laminated Structure: Microstructure and Mechanical Properties," *Materials Today Communications* 40 (2024): 109873.
- 24. J. Chu, L. Tong, Y. Jiang, X. Li, Z. Jiang, and C. Zhang, "Low-Temperature Induced Enhancement of Corrosion/Wear Resistance in Inverse Nacre-Like Graphene-Based Waterborne Coatings," *Applied Surface Science* 657 (2024): 159780.
- 25. Z. Wei, H. Wang, Y. Li, and B. Wang, "Rigidity-Toughness Coupling in Architected Composite Materials for Enhanced Impact Resistance," *International Journal of Mechanical Sciences* 272 (2024): 109191.
- 26. G. Wu, X. Wang, Y. Wang, C. Ji, C. Zhao, and Y. Gao, "Parameter Optimization and Simulation Verification of Polyurea/Ceramic Bionic Staggered Composite Structures," *Materials & Design* 242 (2024): 113008.
- 27. U. Jargalsaikhan, H. Wan, N. Leung, et al., "Micromechanical Modelling for Bending Behaviour of Novel Bioinspired Alumina-Based Dental Composites," *Dental Materials* 40, no. 10 (2024): 1669–1676.

- 28. L. Yuan, S. Xu, M. Chen, Y. Xie, J. Lu, and P. Wang, "Stress Wave in the Mesoscopic Discontinuous Medium by Fractional Approach," *International Journal of Mechanical Sciences* 272 (2024): 109197.
- 29. J. Zeng, Y. Ma, P. Li, et al., "Development of High-Barrier Composite Films for Sustainable Reduction of Non-Biodegradable Materials in Food Packaging Application," *Carbohydrate Polymers* 330 (2024): 121824.
- 30. C. Huang, R. Huang, Y. Cheng, L. Zhao, N. Hu, and Q. Wei, "Strong and Flexible MXene-Based Nanocomposite Films for Atomic Oxygen Resistance and Electromagnetic Interference Shielding," *Composites Science and Technology* 253 (2024): 110665.
- 31. S. Abu-Qbeitah, M. Jabareen, and K. Y. Volokh, "On Strength and Toughness of Soft Staggered Composites," *Mechanics of Materials* 191 (2024): 104935.
- 32. S. Wang, Z. Wang, X. Kong, Y. Sun, and S. Yang, "Ballistic Behavior of Bioinspired Layered-And-Staggered Concrete," *International Journal of Impact Engineering* 191 (2024): 104995.
- 33. X. Xiong, Q. Zeng, Y. Wang, and Y. Li, "Pinning Cracks by Microstructure Design in Brittle Materials," *Journal of the Mechanics and Physics of Solids* 183 (2024): 105497.
- 34. D. Gao, P. Chen, G. Lu, and H. Yang, "Numerical Analysis for Impact Resistance of Nacre-Like Composites," *Materials Today Communications* 35 (2023): 106031.
- 35. S. N. Tiwari and P. K. Agnihotri, "Effect of Freezing Conditions on the Microstructure and Compressive Response of Alumina/Epoxy Nacre-Type Composites," *Materials Today Communications* 37 (2023): 107470.
- 36. G. Wu, X. Wang, Y. Wang, C. Ji, C. Zhao, and Y. Gao, "Blast Response of Bioinspired Nacre-Like Staggered Composite Plates Combined With Steel and Polyurea," *International Journal of Impact Engineering* 180 (2023): 104719.
- 37. Y. Wang, Q. Liu, B. Zhang, et al., "Improved Ballistic Performance of a Continuous-Gradient B4C/Al Composite Inspired by Nacre," *Materials Science and Engineering A* 874 (2023): 145071.
- 38. K. Chen, F. Yang, C. Yao, T. Liu, and H. Jiang, "Single Material FDM Printed Nacre-Like Composite Structure With High Fracture Resistance: Utilizing Interface as Soft Phase," *Composites Communications* 42 (2023): 101682.
- 39. D. Madhav, B. Buffel, P. Moldenaers, F. Desplentere, and V. Vandeginste, "A Review of Nacre-Inspired Materials: Chemistry, Strengthening-Deformation Mechanism, Synthesis, and Applications," *Progress in Materials Science* 139 (2023): 101168.
- 40. A. Sharma, N. K. Shukla, M. O. Belarbi, et al., "Bio-Inspired Nacre and Helicoidal Composites: From Structure to Mechanical Applications," *Thin-Walled Structures* 192 (2023): 111146.
- 41. C. H. Zweben, "Composites: Overview," in *Encyclopedia of Condensed Matter Physics*, ed. F. Bassani, G. L. Liedl, and P. Wyder (Elsevier, 2005), 192–208.
- 42. P. N. B. Reis, P. Sousa, L. M. Ferreira, and C. A. C. P. Coelho, "Multi-Impact Response of Semicylindrical Composite Laminated Shells With Different Thicknesses," *Composite Structures* 310 (2023): 116771.
- 43. M. A. Musthaq Ahamed, H. N. Dhakal, Z. Zhang, A. Barouni, J. R. Pillai, and S. E. Babaa, "Low-Velocity Impact Damage Characteristics of Flax/Glass Epoxy Hybrid Laminates on the Influence of Different Temperatures: Experimental and Numerical Analysis," *Composite Structures* 353 (2025): 118704.
- 44. P. Shabani, L. Li, and J. Laliberte, "Low-Velocity Impact (LVI) and Compression After Impact (CAI) of Double-Double Composite Laminates," *Composite Structures* 351 (2025): 118615.

- 45. J. Baaran, *Study on Visual Inspection of Composite Structures* (European Aviation Safety Agency: European, 2007), 114.
- 46. W. J. Cantwell and J. Morton, "Comparison of the Low and High Velocity Impact Response of Cfrp," *Composites* 20, no. 6 (1989): 545–551.
- 47. C. Yang, Y. Gao, W. Guo, Y. Yang, P. Xu, and M. S. Alqahtani, "High-Velocity Impact Behaviour of Curved GFRP Composites for Rail Vehicles: Experimental and Numerical Study," *Polymer Testing* 116 (2022): 107774.
- 48. Y. Hu, W. Liu, and Y. Shi, "Low-Velocity Impact Damage Research on CFRPs With Kevlar-Fiber Toughening," *Composite Structures* 216 (2019): 127–141.
- 49. T. V. Le, A. Ghazlan, T. Ngo, T. Nguyen, and A. Remennikov, "A Comprehensive Review of Selected Biological Armor Systems—From Structure-Function to Bio-Mimetic Techniques," *Composite Structures* 225 (2019): 111172.
- 50. X. Huang, D. Xiang, G. Xie, et al., "Improving the Impact Resistance of Basalt Fiber-Reinforced Polymer Composites via a Biomimetic Nacre Structure," *Composites Communications* 53 (2024): 102233.
- 51. Z. Wang, Y. Sun, H. Wu, and C. Zhang, "Low Velocity Impact Resistance of Bio-Inspired Building Ceramic Composites With Nacre-Like Structure," *Construction and Building Materials* 169 (2018): 851–858.
- 52. X. Peng and S. Bargmann, "Nacre-Inspired Auxetic Interlocking Brick-And-Mortar Composites," *Composites Communications* 48 (2024): 101892, https://doi.org/10.1016/j.coco.2024.101892.
- 53. Z. Wei and X. Xu, "Gradient Design of Bio-Inspired Nacre-Like Composites for Improved Impact Resistance," *Composites Part B Engineering* 215 (2021): 108830, https://doi.org/10.1016/j.compositesb.2021.108830.
- 54. K. Ko, S. Jin, S. E. Lee, and J. W. Hong, "Impact Resistance of Nacre-Like Composites Diversely Patterned by 3D Printing," *Composite Structures* 238 (2020): 111951, https://doi.org/10.1016/j.compstruct.2020. 111951.
- 55. T. P. Niebel, D. Carnelli, M. R. Binelli, R. Libanori, and A. R. Studart, "Hierarchically Roughened Microplatelets Enhance the Strength and Ductility of Nacre-Inspired Composites," *Journal of the Mechanical Behavior of Biomedical Materials* 60 (2016): 367–377, https://doi.org/10.1016/j.jmbbm.2016.02.008.
- 56. J. Wang, Q. Cheng, and Z. Tang, "Cheminform Abstract: Layered Nanocomposites Inspired by the Structure and Mechanical Properties of Nacre," *ChemInform* 43, no. 17 (2012): 1592–1606, https://doi.org/10.1002/chin.201217216.
- 57. W. Chen, Y. Ma, S. Xu, et al., "Refined Platelet Size: Unlocking Enhanced Mechanics in Nacre-Mimetic Mineralized Materials," *Nano Today* 62 (2025): 102722, https://doi.org/10.1016/j.nantod.2025.102722.